Magnetically induced optical self-pulsing in a nonlinear resonator

F. Mitschke, R. Deserno, W. Lange, and J. Mlynek
Institut für Quantenoptik, Universität Hannover, Welfengarten 1, 3000 Hannover 1, Federal Republic of Germany
(Received 21 October 1985)

We describe a simple nonlinear optical device which transforms an ingoing cw light beam into a periodically modulated one. The mechanism of operation is due to a spin precession in the ground state of optically pumped atoms with a $J=\frac{1}{2}\rightarrow J'=\frac{1}{2}$ transition in the presence of a static transverse magnetic field. With optical feedback from a resonator, this magnetically induced spin precession can be self-sustained and then can give rise to a self-pulsing of the transmitted light at roughly the Larmor frequency. A detailed theoretical description of the system is presented and stability criteria are considered. In contrast to earlier work, our calculations take into account the resonator round-trip time, an optical detuning from the atomic resonance, and absorptive losses within the resonator. New signal features are predicted: These include a complicated structure of the initial transient as well as a precipitation to a stationary state. Our theoretical model is confirmed by measurements which are performed by means of a Fabry-Perot resonator containing sodium vapor. The behavior of the device is studied for a wide range of experimental parameters; threshold powers for oscillation ($\gtrsim 5$ mW) and the oscillation frequency and its tuning range (140 kHz–13 MHz) are investigated as well as the dynamics of the system following a step input of light.

I. INTRODUCTION

Nonlinear dissipative systems with at least two degrees of freedom may exhibit limit cycle oscillations. In this communication we will discuss such a system from the viewpoint of optics. Our device transforms an ingoing cw light beam into a periodically modulated output beam, a process called optical self-pulsing. This process occurs in the interaction of a light field and an atomic $J=\frac{1}{2}\rightarrow J'=\frac{1}{2}$ transition inside an optical resonator in the presence of an external static magnetic field (see Fig. 1). Optical pumping gives rise to an orientation of the atomic spins in the $J=\frac{1}{2}$ ground state; the magnetic field causes the spins to precess, and this precession is self-sustained due to optical feedback. As the oscillation frequency is essentially given by the Larmor frequency, it can easily be tuned by simply varying the magnetic field.

A device capable of producing tunable optical self-oscillations is certainly interesting in view of possible technical applications. On the other hand, a good deal of motivation for the study of such a device stems from the now widespread interest in "self-organizing" systems in the context of synergetics.

Optical self-oscillations have been discussed in the literature before: McCall[1] showed that an optical bistable device can develop self-pulsations if the nonlinearity contains two contributions of opposite sign and with different time constants (one of these usually being thermal). Systems based on this concept[2,3] have the disadvantage that they are not easily tuned, in marked contrast to the system we describe here.

The mechanism of magnetically induced self-sustained spin precession was predicted by Kitano, Yabuzaki, and Ogawa (KYO) in Ref. 4 and observed for the first time by Mitschke, Mlynek, and Lange in a sodium-filled Fabry-Perot resonator.[5] In the present work we give an advanced formal description of the phenomenon and compare our theory to more detailed experimental results. After a phenomenological description of the mechanism (Sec. II), a detailed theoretical analysis is given in Sec. III. In contrast to the theoretical approach used by KYO, our treatment also includes the finite resonator round-trip time, absorptive losses, and effects due to the atomic detuning. Results from numerical calculations are given in Sec. IV. In Sec. V we present the experimental work which is again performed with the use of a sodium-filled Fabry-Perot resonator. As will be seen then, our theoretical results are in good agreement with the experimental findings.

II. THE PRINCIPLE OF OPERATION

Our description is based on a representation of the active medium as an ensemble of $J=\frac{1}{2}$ atoms. We are thus concerned with a four-level system as shown in Fig. 1. In the following discussion we will assume that excited-state populations are always small and that sublevel coherence within the excited state can be neglected. Now let us first suppose that only circularly polarized light (either σ_+ or σ_-) is present; thus only one of the transitions $1\rightarrow 4$ or $2\rightarrow 3$ is excited. This excitation will, in connection with the spontaneous decay of the upper levels (decay rate Γ_1) create a ground-state population difference, or orientation, w. This orientation, which corresponds to an atomic spin polarization in the $J=\frac{1}{2}$ ground state, is counteracted by its decay rate γ. If $\Gamma_1/\gamma \gg 1$, w saturates at an intensity which is far less than the saturation intensity for the optical transition in a pure two-level system with decay rate Γ_1. The optical pumping thus gives rise to a strong nonlinearity already at low intensity, a well-known fact which

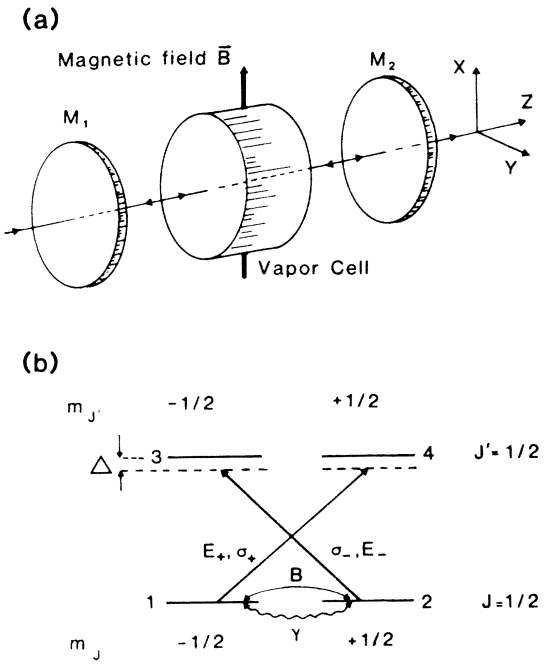

FIG. 1. (a) Simplified geometry of the vapor-filled Fabry-Perot resonator with mirros M_1 and M_2. The nonlinear medium is subjected to a static transverse magnetic field. (b) Schematic of the atomic $J=\frac{1}{2}\rightarrow J'=\frac{1}{2}$ transition, interacting with σ_+ and σ_- light; the quantization axis coincides with the propagation direction of light (z axis). The static magnetic field B can induce transitions between the degenerate ground-state Zeeman levels with γ denoting the corresponding relaxation rate. The optical detuning is given by Δ. Excited-state effects are neglected.

has been utilized to demonstrate, e.g., low-threshold optical bistability.[6]

If, on the other hand, linearly polarized light is irradiated, the two optical pumping processes due to σ_+ and σ_- light are in competition with each other. Due to the symmetry of the level scheme, they would mutually cancel and no orientation would arise if both processes were independent of each other. This independence means that the absorption coefficient and the refractive index for one transition are not affected by the intensity acting on the other transition. For very low intensities, this condition is obviously fulfilled, and no net optical pumping will occur. The symmetry of the system is thus retained; we will call this state the symmetrical one. The independence of both pumping processes can, however, be lost in the saturation regime. This is best seen as follows: Assume that the intensities for both transitions are slightly different for a short moment, e.g., due to fluctuations. A momentarily dominant σ_+ light will result in reduced absorption for the corresponding transition and an increased absorption for the other transition. Also, the refractive indices would be different in the case of nonvanishing optical detuning Δ; for the moment, however, let us assume perfect tuning of the light field to the atomic resonance.

Now the optical feedback comes into action: under its influence, the imbalance will be increased, because the wave that is transmitted more strongly is also fed back more strongly. One concludes that while the symmetric state is always an equilibrium state, its stability is lost for certain intensity ranges. Fluctuations can break the symmetry, and eventually the system reaches an asymmetric state where light for one transition is highly transmitted, while for the other transition one finds strong absorption.

Obviously, there are two such asymmetric states in addition to the symmetric one. In the symmetric state, the transmitted light field in the output remains linear, like the input light field, but in the asymmetric states it is essentially circularly polarized, either to the left or to the right. This can also be described in terms of the orientation of the atomic spins: While the spins are oriented at random in the symmetrical state, they are parallel to the light propagation direction in one and antiparallel to it in the other asymmetric state. This means that there is a macroscopic spin polarization and, as a consequence, a macroscopic magnetization present in the asymmetric states.

What we have described so far is an absorptive effect, but the dispersive counterpart also exists. If the light field has a frequency detuning with respect to both the atomic and cavity resonances, the intensity-dependent refractive index comes into play. It causes intensity-dependent phase shifts of the light field, which in turn are transformed into intensity changes by virtue of the interference in the resonator. This dispersive effect has been reported before, and the property of having three stable states is referred to as "optical tristability;"[5,7,8] the change of polarization state of the transmitted light field in the symmetry-breaking transition has been termed "polarization switching."[9] Throughout this paper, we will in fact concentrate on the dispersive effects.

Now consider the influence of a transverse magnetic field B on the ground-state spins in this optically pumped system (see Fig. 1). The B field makes the spins, or the magnetization, precess around the B-field direction with the Larmor frequency $\Omega_L \sim B$. The spin precession can be detected in the output intensities of the two circular polarization components: they are modulated at the precession frequency with opposite phase. Without optical feedback, these modulations would damp out due to ground-state relaxation processes. With suitable optical feedback applied, the precession may be undamped, or self-sustained. One requirement for this occurrence is that the precession of the magnetization is much faster than its relaxation. When the magnetization rotates so far that its component along the optical axis changes sign before being damped out considerably, it can be reinforced again by the polarized light field.

III. THEORY

We consider the behavior of a system consisting of atoms in a resonator with an incident radiation field of well-defined polarization, tuned to a $J=\frac{1}{2}\rightarrow J'=\frac{1}{2}$ transition in the presence of a static transverse magnetic field B. In this section we present a brief outline of the theoretical description; for details the reader is referred to Appendixes A and B.

A. Equations for the nonlinear medium

The time evolution of the atomic system can semiclassically be described by the equation of motion for the density matrix

$$i\hbar\dot{\rho}=(\mathscr{H}_0+\mathscr{H}_B+\mathscr{H}_E,\rho) . \tag{1}$$

Here $\mathscr{H}_0$ denotes the Hamiltonian of the atomic system without external fields, $\mathscr{H}_B$ and $\mathscr{H}_E$ represent the interaction of the atoms with the magnetic field B and the light field E, respectively. Since we treat the direction of propagation of the light beam as the quantization axis, $\mathscr{H}_E$ couples the levels 1 and 4 (σ_+ light) and 2 and 3 (σ_- light) and gives rise to optical coherences ρ_{14} and ρ_{23}. The magnetic field is assumed to be transverse; it couples levels 1 and 2 and levels 3 and 4 and gives rise to Zeeman coherences ρ_{12} and ρ_{34}. The simultaneous presence of E and B creates coherences between levels 1 and 3 and levels 2 and 4. Moreover, the population densities of the four levels, which are represented by the diagonal elements of ρ, have to be taken into account. Finally, relaxation terms have to be added to Eq. (1).

Under the conditions of the experiment several simplifying assumptions can be made in solving Eq. (1) (see Appendix A): (i) The relaxation of the optical coherences ρ_{13}, ρ_{24}, ρ_{14}, and ρ_{23} is assumed to be fast with respect to all changes of field amplitudes, thus these quantities can adiabatically be eliminated. As a consequence, the influence of the radiation field on populations and Zeeman coherences can be described by transition rates. (ii) The optical transition is assumed to be homogeneously broadened, i.e., the Doppler effect is neglected. (iii) The population of the excited state and the Zeeman coherence within the excited state are neglected, i.e., $\rho_{11}+\rho_{22}\simeq 1$, $\rho_{34}\simeq 0$. (iv) The ground-state Larmor frequency Ω_L is assumed to be small compared to the optical linewidth Γ_2, i.e., $\Omega_L \ll \Gamma_2$. (v) The Zeeman coherence and the population densities in the ground state are assumed to decay with equal time constants $1/\gamma$ to their equilibrium values.

Under these assumptions the remaining variables are $\rho_{11}-\rho_{22}$, representing the difference of populations in the Zeeman sublevels of the atomic ground state, and ρ_{12}, representing the coherence between the Zeeman sublevels. It is convenient to define a Bloch vector $\mathbf{m}=(u,v,w)$ by

$$u=\rho_{12}+\rho_{21},\quad v=i(\rho_{12}-\rho_{21}),\quad w=\rho_{11}-\rho_{22} , \tag{2}$$

whose components are related to the expectation values $\langle s_i\rangle$ of the spin components by $\frac{1}{2}\hbar\,|m_i|=|\langle s_i\rangle|$. In Appendix A it is shown that the temporal dependence of m is described by the following equations:

$$\dot{u}=-(P_++P_-+\gamma)u-(P_--P_+)\bar{\Delta}v , \tag{3a}$$

$$\dot{v}=-(P_++P_-+\gamma)v+(P_--P_+)\bar{\Delta}u-\Omega_L w , \tag{3b}$$

$$\dot{w}=-(P_++P_-+\gamma)w+\Omega_L v+(P_--P_+) . \tag{3c}$$

Here P_+ and P_- represent pump rates introduced by the σ_+ and σ_- light, respectively, and $\bar{\Delta}=(\omega_0-\omega)/\Gamma_2$ is related to the detuning of the laser frequency ω with respect to the atomic resonance frequency ω_0. Equations (3a)–(3c) can also be written as a Bloch-type equation

$$\dot{\mathbf{m}}=\mathbf{\Omega}\times\mathbf{m}-\gamma_{\text{eff}}\mathbf{m}+\mathbf{P} , \tag{4a}$$

with

$$\mathbf{\Omega}=(\Omega_L,0,(P_--P_+)\bar{\Delta}) , \tag{4b}$$

$$\mathbf{P}=(0,0,P_--P_+) , \tag{4c}$$

$$\gamma_{\text{eff}}=P_++P_-+\gamma . \tag{4d}$$

In the absence of light Eq. (4a) describes the precession of $\mathbf{m}$ with angular frequency Ω_L around the magnetic field; the amplitude of $\mathbf{m}$ decays exponentially with the decay constant γ in this case. In the presence of light the damping term γ_{eff} is increased, but simultaneously a source term is present, provided that $P_+\neq P_-$. It should be noted that in the case of unequal σ_+ and σ_- intensities ($P_+\neq P_-$) and off-resonant optical excitation ($\bar{\Delta}\neq 0$), $\mathbf{\Omega}$ does not coincide with the direction of the magnetic field. This represents a major difference in the analysis of KYO, who omit the term $(P_--P_+)\,\bar{\Delta}$ in Eq. (4b). Physically, this term can be interpreted as a light-shift effect on the ground-state sublevels that clearly shows up in the response of the sublevel coherence to a step input of light: the oscillation frequency of this initial transient (in the absence of optical feedback) is given by $\Omega=[\Omega_L^2+(P_--P_+)^2\bar{\Delta}^2]^{1/2}$. Detailed experimental and theoretical studies of this novel optically induced spin nutation will be published elsewhere.[10]

In Appendix A it is further shown that the absorption coefficient α_0 and the refractive index n_0 of the unpolarized medium have to be replaced by polarization dependent quantities if the w component is nonvanishing. Referring to σ_+ and σ_- light, we find

$$\alpha_\pm=\alpha_0(1\pm w) , \tag{5}$$

$$n_\pm=1+(n_0-1)(1\pm w) . \tag{6}$$

In the next subsection it will become obvious that P_+ and P_- are not constants but functions of w as soon as one takes optical feedback into account.

B. The resonator equation

The optical feedback is achieved by placing the nonlinear medium inside a cavity. In our experiment we use a Fabry-Perot resonator, i.e., a standing-wave device [see Fig. 1(a)]. Although this configuration is experimentally very convenient, a corresponding theoretical treatment is strongly complicated by the intensity modulation through the medium. In our model we thus prefer to use a ring cavity, i.e., the simplest geometry, with fields circulating in a single direction. In fact, a strong influence of standing-wave effects on our experimental results was ruled out by repeating part of the experiments in a ring cavity; the signal forms were observed to be essentially the same as in the Fabry-Perot experiment. This is not surprising because under our experimental conditions the atoms move many wavelengths during the pumping time $1/P_\pm$, or the decay time $1/\gamma$; consequently, the z dependence of the relevant atomic variables (u,v,w) due to the standing-wave structure of the pumping fields should be essentially washed out.

The equation relating incident and intracavity field amplitudes for a ring cavity containing the atomic medium is determined from Maxwell's equations together with appropriate boundary conditions. We assume plane waves and a slowly varying field envelope. Let $\mathscr{L}$ be the resonator length and L the length of the nonlinear sample with $L \ll \mathscr{L}$. Taking into account the time delay $t_R = \mathscr{L}/c$ due to the propagation, we find in the mean-field limit for the normalized intracavity field amplitude $p_\pm(t)$ ($|p_\pm|^2 = P_\pm$) at time t and at $z=0$ (see Appendix B):

$$p_\pm(t) = \sqrt{1-R_f}\,p_{I,\pm}(t) + \sqrt{R_f R_b}\,p_\pm(t-t_R) \times \exp\{-L\alpha_\pm(t-t_R) - i[\phi_\pm(t-t_R)+\phi_0]\} . \tag{7}$$

Here $p_{I,\pm}(t)$ denotes the normalized incident field amplitude and $k=\omega/c$. R_f (R_b) is the front (back) mirror intensity reflectivity, ϕ_0 describes a constant phase shift, and $\phi_\pm = n_\pm kL$. For our numerical calculations we will assume t_R to be nonzero, but very small compared with $1/\gamma$; this rules out delay-induced instabilities of the Ikeda type.[11]

Equations (3)—(7) constitute our model, which serves to describe the time evolution of the system with optical feedback. There are three major differences with the earlier model of KYO. First, KYO implicitly assume a broadband excitation; consequently, the terms proportional to $\bar{\Delta}$ in Eq. (3) do not appear. Note that with these terms included, the second of Eqs. (3a)—(3c) is coupled to the other ones which makes the system three dimensional. Second, we consider absorptive effects in Eqs. (5) and (7). Third, our resonator equation includes the finite resonator round-trip time t_R. In the numerical solutions of Eqs. (3)—(7) we present below, it will become evident that all three distinctions have consequences for the behavior of the system. Let us first analyze, however, the stability of the steady state of the system.

C. Stability analysis

In the stationary state we can set $\dot{u}=\dot{v}=\dot{w}=0$ and $p_\pm(t)=\text{const}$; in this case the resonator equation is simplified and can be replaced by an Airy function [see Eq. (B11)]. We first calculate the steady-state solutions of Eqs. (3a)—(3c). With the definitions $S=(P_-+P_+)/\gamma$, $D=(P_--P_+)/\gamma$, and $\bar{\Omega}_L=\Omega_L/\gamma$ and by denoting the stationary values by an index s, we find

$$u_s = \frac{D_s\bar{\Omega}_L}{(S_s+1)^2+D_s^2\bar{\Delta}^2+\bar{\Omega}_L^2}\,\frac{D_s\bar{\Delta}}{S_s+1} , \tag{8}$$

$$v_s = -\frac{D_s\bar{\Omega}_L}{(S_s+1)^2+D_s^2\bar{\Delta}^2+\bar{\Omega}_L^2} , \tag{9}$$

$$w_s = \frac{(S_s+1)^2+D_s^2\bar{\Delta}^2}{(S_s+1)^2+D_s^2\bar{\Delta}^2+\bar{\Omega}_L^2}\,\frac{D_s}{S_s+1} . \tag{10}$$

For simplicity let us assume in the following the case of linear input polarization; then one has $P_{I,+}=P_{I,-}$, and $u_s=v_s=w_s=0$ is always a fixed point because for $w=0$, also $\alpha_+=\alpha_-$, $n_+=n_-$, and $D=0$. We will now investigate the stability of this fixed point.

After linearization of Eqs. (3a)—(3c) around $u_s=v_s=w_s=0$, one finds the characteristic equation for the eigenvalues λ of the problem:

$$\lambda^3+\lambda^2[3(S_s+1)-D_s'] + \lambda[3(S_s+1)^2-2(S_s+1)D_s'+\bar{\Omega}_L^2] + (S_s+1)[(S_s+1)^2-(S_s+1)D_s'+\bar{\Omega}_L^2]=0 . \tag{11}$$

Here $D_s'=dD/dw\,|_s$ stems from the Taylor expansion of $D(w)$ around $w=w_s$. The solutions of Eq. (11) are given by

$$\lambda_1 = -(1+S_s) , \tag{12a}$$

$$\lambda_{2,3} = -(1+S_s)+\tfrac{1}{2}D_s' \pm \tfrac{1}{2}(D_s'^2-4\bar{\Omega}_L^2)^{1/2} . \tag{12b}$$

If the expression under the root is positive or zero, the eigenvalues are real and no oscillations can occur; for any of the $\lambda_i>0$, switching may occur.

If the argument of the root is negative, there are two complex eigenvalues giving rise to oscillatory motion; the oscillations are undamped if the real part is positive, or

$$D_s'/(1+S_s) \geq 2 . \tag{13}$$

This expresses a sort of minimum differential gain for oscillations. The condition that the root be complex yields $\bar{\Omega}_L \geq |D_s'/2|$; this is a minimum magnetic field for oscillations. It follows from the last two expressions that a minimum Larmor frequency

$$\bar{\Omega}_{L,\min} \geq 1+S_s \tag{14}$$

is required for oscillatory motion to occur. Finally, the oscillation frequency $\bar{\Omega}_0=\Omega_0/\gamma$ is determined by the imaginary part of the eigenvalues. Assuming $2\bar{\Omega}_L \geq D_s'$, $\bar{\Omega}_0$ is given by

$$\bar{\Omega}_0 = \bar{\Omega}_L\left[1-\left[\frac{D_s'}{2\Omega_L}\right]^2\right]^{1/2} . \tag{15}$$

The frequency of the large amplitude oscillations may well be different.

The conditions for switching and oscillations can now be found by calculating D_s' from the resonator equation which in the limit $t_R \to 0$ is given by an Airy function [see Eq. (B11)]. With the use of the Airy function, Eqs. (13)—(15) can be applied to the dispersive and absorptive case separately.[12] One finds, however, that in the absorptive case the conditions for oscillation require a violation of previously made assumptions (optically thin medium, power not too high so that the population in the optically excited state is negligible). At this point we may already mention that in the experiment we never found oscillations under absorptive conditions.

In the case of circular input polarization a stability analysis is more difficult to perform. On inspection of Eq. (4) it is plausible, however, that oscillations can also occur in that case. The pumping rates enter the Eqs. (3a)—(3c) in two places: (i) they appear in the dissipation term $\gamma_{\text{eff}}=(\gamma+P_++P_-)$, but a reduction of dissipation by setting either P_+ or P_- equal to zero will hardly quench the oscillations. (ii) They are present in the driving term P_--P_+. It is essential that this term not be

zero all the time. We thus expect oscillations to occur not only in the case of linear input polarization but also for circular or elliptical polarization.

IV. NUMERICAL RESULTS

The complete set of time-dependent equations (3)—(7) can only be solved numerically. We will consider the response of the system to a sudden switch-on of the input intensity, i.e., the initial transient and the evolution towards equilibrium. In particular, we compute the trajectory of the Bloch vector in the (u,v,w) space, visualized as projections onto the (u,w) and the (v,w) plane. For a comparison with the experiment we also calculate the quantities $P_{T,+}$ and $P_{T,-}$ that are related to the intracavity pumping rates $P_{\pm}$ by $P_{T,\pm}=P_{\pm}(1-R_b)\exp(-2\alpha_{\pm}L)$; $P_{T,+}$ and $P_{T,-}$ are proportional to the two detector signals monitored in our experiment (see Sec. V).

With circular input polarization ($P_{I,+}$ or $P_{I,-}$ equals zero) we find transient bistable switching with critical slowing down for absorptive, dispersive, and mixed cases. For linear input polarization ($P_{I,+}=P_{I,-}$), tristable switching is found in a very similar fashion; here, the symmetry breaking due to small fluctuations is simulated choosing slightly different starting values for $P_{I,+}$ and $P_{I,-}$. Both absorptive and dispersive tristability can be obtained. In the dispersive case and with a sufficiently large magnetic field, there is an interval of intensities where self-oscillations occur. This is true for arbitrary polarization states of the input light; we will, however, in the following concentrate on the case of linear polarization.

At the low-intensity end of this interval with self-oscillations, the oscillations build up very slowly and the stationary amplitude is approached monotonously. In the phase-space projection to the (v,w) plane, this corresponds to a trajectory spiraling out from the origin and smoothly approaching the limit cycle without crossing it. With increased intensity, the amplitude buildup is faster, and the envelope has an "overshoot" [Fig. 2(a)]. In the projection to the (v,w) plane, the trajectory spirals further out and then approaches the limit cycle from the outside [Fig. 2(b)]; for illustration, Fig. 2(c) shows the corresponding projection to the (u,w) plane. In the (u,v,w) space the trajectory does not intersect itself, of course. Note that such an overshooting behavior is only possible in a phase space of more than two dimensions. With a further increase in intensity, the oscillations finally stop abruptly, and the system remains at one of the asymmetric states that already occurred in tristable switching (Fig. 3). If in this regime the intensity is adjusted very carefully, one finds narrow intervals with very complicated "staggering" behavior in the inital stage of the oscillations, which eventually reaches either the limit cycle or one of the two asymmetric fixed points. An example for the first case is shown in Fig. 4. Let us mention that whether a fixed point or the limit cycle is approached also depends on initial conditions.

The linear stability analysis presented above does not predict this precipitation of the oscillations at high intensities, of course, because it can only describe a small vicinity of the unstable fixed point. It also fails to predict the existence of an upper limit for the oscillation frequency, a feature due to the finite round-trip time of the resonator. It is clear that if the intracavity photon lifetime is longer than the oscillation period, the oscillations are strongly damped.

An estimate for the upper frequency limit can best be made as follows: In the time domain, we are concerned with a light field of oscillating intensity. This corresponds, in the frequency domain, to a "carrier" at the optical frequency with two (or more, for the harmonics)

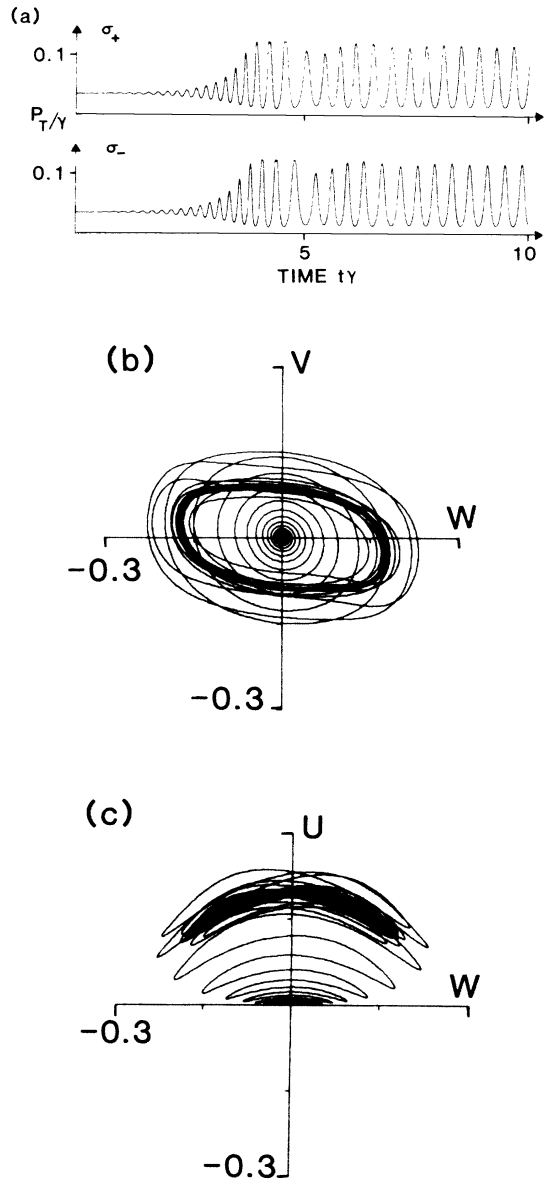

FIG. 2. The onset of magnetically induced self-pulsing after a sudden switch-on of the input intensity at $t=0$. (a) The calculated σ_+ and σ_- polarization components of the cavity output P_T vs time $t\gamma$. (b) and (c) The projections of the Bloch vector $\mathbf{m}=(u,v,w)$ on the (v,w) and (u,w) planes, respectively. Parameter values for (a)—(c) are $P_{I,\pm}/\gamma=0.408$, $\Omega_L/\gamma=30$, $\Delta/\Gamma_2=20$, $\alpha_0 L=0.124$, $\phi_0=-0.5$, $R_f=0.7$, $R_b=0.9$, and $t_R\gamma=5\times10^{-4}$; number of time values on the abscissa is 20 000.

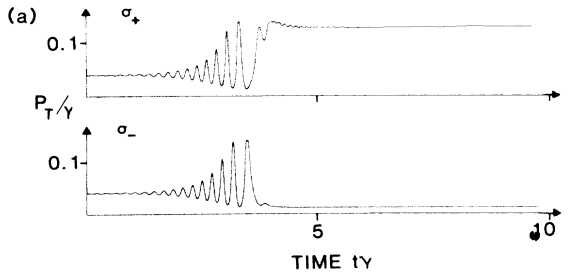

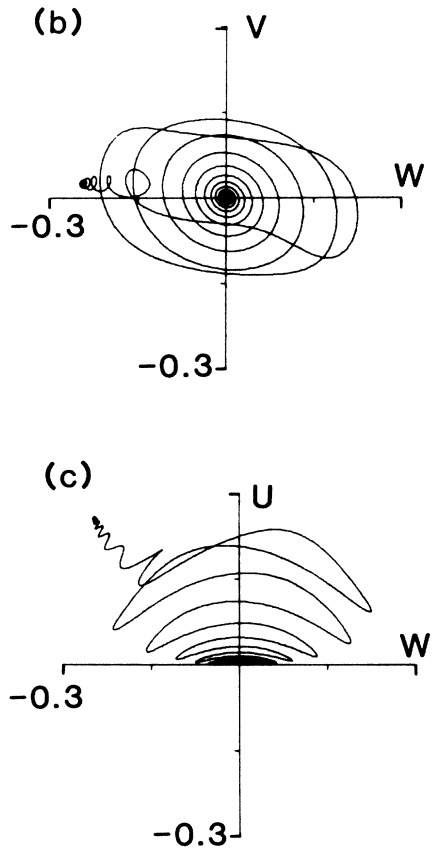

FIG. 3. The stopping of oscillations at a somewhat higher pumping rate ($P_{I,\pm}/\gamma=0.464$) as compared to Fig. 2; otherwise parameters as in Fig. 2. (a) The cavity output $P_{T,\pm}/\gamma$ vs time $t\gamma$. (b) and (c) The projections of the Bloch vector on the (v,w) and (u,w) plane, respectively, showing the approach to an asymmetric fixed point.

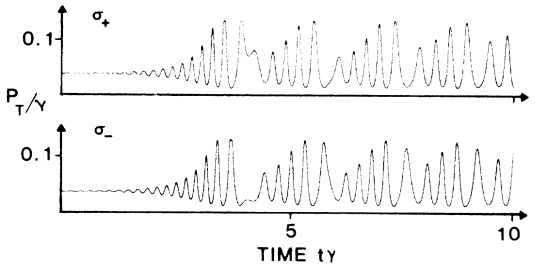

FIG. 4. A typical staggering transient, eventually reaching a limit cycle. $P_{I,\pm}/\gamma=0.446$; otherwise parameters as in Fig. 2.

sidebands, at a distance equaling the oscillation frequency. For small oscillation frequencies, the distance between the sidebands may be small compared with the resonance width of the resonator. In that case, all spectral lines are enhanced by constructive interference. For higher frequencies, however, at least one of the sidebands inevitably is suppressed in the wing of the Airy peak. Consequently, the self-sustained oscillation is quenched. One estimates that the frequency distance between the sidebands should be of the order of the half-width at half maximum of the Airy peak. This yields $\Omega_{0,\max}\simeq\pi c/(4L\mathcal{F})$, with $\mathcal{F}$ denoting the cavity finesse. Numerical results show that indeed for Larmor frequencies in the order of this estimate the waveform of the oscillations becomes more sinusoidal, and also that the oscillation amplitudes shrink. For somewhat higher Larmor frequencies the oscillations finally disappear altogether.

We summarize and note that a comparison of our theory with the earlier one from KYO reveals three major modifications. First, including the terms proportional to $\bar{\Delta}$ in Eq. (3) makes the phase space three dimensional which in turn gives rise to the prediction of a complicated behavior in the initial transient. Second, the inclusion of the finite resonator round-trip time brings about an upper limit for the oscillation frequencies, and also more complicated dynamics in the vicinity of the asymmetric fixed points. Third, taking absorption losses into account strongly influences the waveform of the oscillations. Figure 6 of KYO is a typical result from a calculation with no absorption taken into account; in contrast, our calculated signals can display a much smoother and more symmetrical shape (see Fig. 5).

Let us finally comment on the complicated staggering behavior in the initial transient at intensities near the upper intensity limit for oscillations. During this transient, the motion is nonperiodic and can be highly irregu-

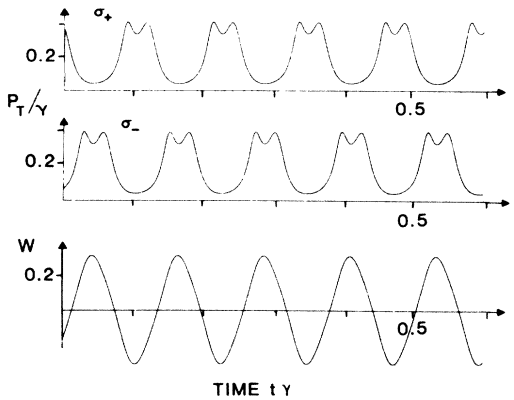

FIG. 5. Self-pulsing in the σ_+ and σ_- components of the transmitted light on a small time scale. $P_{T,\pm}/\gamma$ is displayed as a function of time together with the time evolution of the ground-state population difference w. Parameters are $P_{I,\pm}/\gamma=3$, $\Omega_L/\gamma=20$, $\Delta/\Gamma_2=8$, $\alpha_0 L=0.3$, $\phi_0=-0.5$, $R_f=0.7$, $R_b=0.9$, and $t_R\gamma=10^{-4}$; number of time values on the abscissa is 6000.

lar. It has also been shown that two trajectories which are initially very close to each other rapidly diverge exponentially until they reach macroscopically distant parts of the phase space.[12] This is strongly reminiscent of the so-called "chaotic transients" discussed in the literature.[13,14] The occurrence of chaotic transients may be taken as a hint that in their vicinity (in parameter space) continued chaotic motion may occur. With this in mind, we surveyed this vicinity in numerical experiments and found that with a slight increase in t_R from $t_R\gamma\simeq 10^{-4}$ used above to between 10^{-2} or 10^{-3} (which is still small), the asymmetric fixed points may become unstable, too. Each of them then undergoes a sequence of period-doubling bifurcations towards chaos. Finally, transitions between the two chaotic attractors appear; we note that similar transitions have been predicted for a somewhat related optical system.[15] There is reason to believe that the whole behavior can approximately be described by the one-dimensional map $x_{n+1}=a\sin(\pi x_n)$ in the regime from $a=0$ to $a\geq 1$. More detailed work on this aspect of our system is in progress.

V. EXPERIMENTS

In this section we will present the experimental work which was performed with the use of a sodium-filled Fabry-Perot resonator. We also compare the experimental findings to our theoretial predictions.

A. The experimental setup

Let us first outline the essentials of the apparatus (see Fig. 6), which is an improved version of the setup described in Ref. 5. The probe material is contained in a heated ceramic tube of 10 mm diameter, the length of the heated zone being 40 mm. The tube ends are cooled and, by flexible bellows, connected to the resonator mirrors which also seal the vacuum chamber; we thus avoid windows internal to the resonator. The resonator is about 15 cm long and nearly confocal, the beam waist being 120 μm. Mirror coatings are chosen such as to give a finesse of about 15 (without sodium). The mirror distance is defined by quartz rods for thermal stability, with a possibility for fine adjustment with a piezo translator.

The light source is a free-running single-mode cw dye ring laser. Optical isolation from the experiment is achieved by a 45° Faraday rotator in connection with two polarizers. The beam is approximately mode matched into the resonator with the help of a suitable lens. Polarizing optics and/or an electro-optic modulator may be placed in the input beam if one desires to choose certain polarization states or to control the input intensity. Signal detection includes a $\lambda/4$ plate, a Wollaston prism, and two photodiodes of the same type for monitoring the two counterrotating circularly polarized fields separately. The signals are first stored in a Datalab DL 922 transient digitizer; they may then be photographed or further processed by a microcomputer.

As a probe material, we employ sodium vapor. Typically, sodium number densities of 10^{12} to 10^{13} cm^{-3} are used, and the laser is tuned to the D_1-resonance line. The transverse magnetic field B is created by a pair of

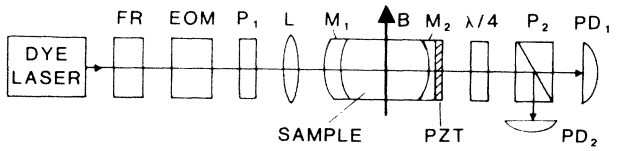

FIG. 6. Schematic of the experimental setup. FR, Faraday rotator; EOM, electro-optic modulator; P_1, polarizer or $\lambda/4$ plate; L, mode matching lens; M_1, scanning lens; B, transverse static magnetic field; M_2, rear mirror; PZT, piezoelectric translator; $\lambda/4$, quarter-wave plate; P_2, polarizing analyzer; $PD_{1,2}$, photodiodes.

Helmholtz coils; the Earth's magnetic field is compensated for by means of additional coils. In a weak field B, the hyperfine interaction strongly affects the ground-state Zeeman coupling and thus has to be taken into account in the evaluation of the Larmor frequency. With nuclear magnetism being neglected, the Landé g_F factors for the two hyperfine levels only differ by sign ($|g_F|=0.5$), and the Larmor frequency is thus given by $\Omega_L=2\pi(7.00\text{ MHz})B/\text{mT}$.

In the experiments argon buffer gas is added to the sodium vapor at a pressure of 200 mbar. The corresponding pressure broadening of the resonance line of about 3 GHz (FWHM) thus masked the ground-state hyperfine splitting (1.8 GHz) as well as the Doppler broadening (1.6 GHz). Moreover, the $^2P_{1/2}$ excited-state orientation is rapidly destroyed by collisions whereas the $^2S_{1/2}$ ground-state orientation is rather insensitive to collisions, thus allowing efficient optical pumping.[16] In our theoretical model, we strongly simplify the overall optical excitation process: hyperfine pumping is completely ignored, and we model the sodium vapor as an essentially homogeneously broadened $J=\frac{1}{2}\rightarrow J'=\frac{1}{2}$ atomic system with excited-state effects being neglected.

The relevant decay rate γ corresponds to the decay time of the $^2S_{1/2}$ ground-state orientation which is mainly destroyed by collisions with the cell wall. With respect to our signal formation, γ is determined by the transit time of the optically pumped atoms through the laser beam; in the presence of buffer-gas atoms, the motion of the Na atoms is diffusive. For our purpose the decay time of the orientation found within the interaction region can be represented reasonably well by a single time constant $1/\gamma$ of the order $\gamma^{-1}\simeq r^2/4D$;[17] here r is the beam radius and $D=\bar{v}\kappa/3$ denotes the diffusion constant, κ is the mean-free-path length, and $\bar{v}$ is the average thermal velocity. For our experimental situation with $r\simeq 0.12$ mm and $D\simeq 3.5$ cm^2/s, we find $\gamma^{-1}\simeq 10$ μs. This estimate was confirmed in an independent experiment where the decay time of w was measured directly.

B. Experimental results and discussion

As explained above, for circular input polarization and a very small magnetic field one can observe optical bistability. Thresholds for switching of 1.2 mW have been observed for dispersive bistability, with somewhat higher

values in the absorptive case (i.e., with both atomic and resonator detuning being zero). With linear input polarization, we obtain optical tristability at intensities from 2 mW on in the dispersive case [Fig. 7(a)] and again slightly higher values for the absorptive case. In the asymmetric polarization state, the ratio of the two detector signals may exceed 10^3.

With a transverse magnetic field, all switching thresholds are shifted towards higher intensities. For fields larger than about 0.03 mT, self-pulsation may occur [Fig. 7(b)] if the light intensity is not less than 5 mW. This also requires an atomic detuning of 5–15 GHz which is, however, uncritical. Also, the minimum required number density of the sodium vapor is somewhat higher than for bistability; this is the main reason that self-oscillations were not observed in a previous study of optical bistability.[18] As mentioned above, we were not able to produce self-pulsations close to the line center (absorptive case). Under dispersive conditions oscillations are observed for circular, elliptical, and linear polarization of input light. But for the sake of clarity, we will again concentrate on the case of linear input polarization.

According to Eq. (14), the lowest possible magnetic field should be determined by the ground-state relaxation rate γ. The lowest observed frequency for self-pulsations of $\Omega_0=2\pi(140\text{ kHz})$ is in rough agreement with the value of 1/10 μs given above. We have also checked the fact that with a resonator with a larger beam waist and thus smaller γ, the oscillations can be obtained at much lower frequency, down into the audio range.

The pulse shape strongly depends on the parameters. For a wide choice of parameter values, two maxima are observed in each pulse; this feature is shown in Fig. 8, where the self-pulsing is displayed on a shorter time scale. It should be noted that our calculated wave form in Fig. 5 clearly matches this experimental result. For increasing magnetic field, the waveform of the oscillations becomes more sinusoidal, and for magnetic fields larger than about 1 mT, the amplitudes of the oscillations decrease, and finally the oscillations disappear altogether. The highest observed oscillation frequency was $\Omega_0=2\pi(13\text{ MHz})$, which is again of the order of the value estimated from $\Omega_{0,\max}\simeq\pi c/(4L\mathcal{F})$ (see Sec. IV) with $L=15$ cm and $\mathcal{F}\simeq 15$ [$\pi c/(4L\mathcal{F})\simeq 2\pi(17\text{ MHz})$]. Thus, there were no oscillations at all whenever the Larmor frequency was outside the range given in Secs. II and III.

The intensity threshold for the onset of oscillations was found to be nearly independent of the magnetic field over most of the tuning range. This is in accord with Eq. (13) and with our numerical results. Below threshold, damped

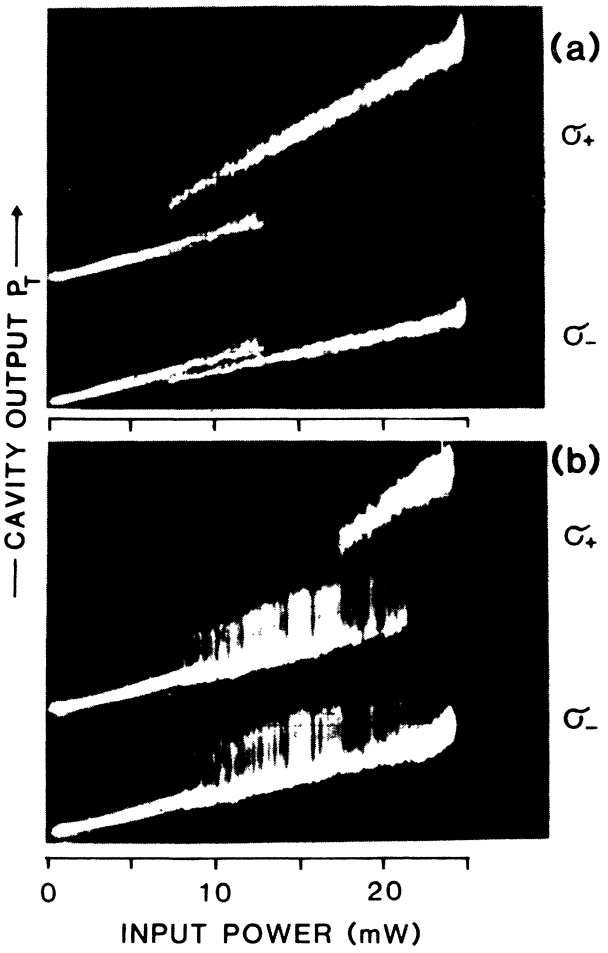

FIG. 7. Experimental recordings of hysteresis cycles as the input power is scanned forth and back. The ordinate displays the signals of the two photodiodes PD_1 and PD_2 which monitor the σ_+ and σ_- components of the cavity output, respectively; the two traces are separated vertically for clearness. (a) No magnetic field applied. (b) $B=0.06$ mT [$\Omega_L=2\pi(400\text{ kHz})$]; the self-oscillations appear as shaded area. Other experimental parameters in (a) and (b) are $\Delta\simeq 2\pi(5\text{ GHz})$, $N_{Na}\simeq 10^{12}$ cm^{-3}, and $p_{Ar}\simeq 200$ mbar; linear input polarization.

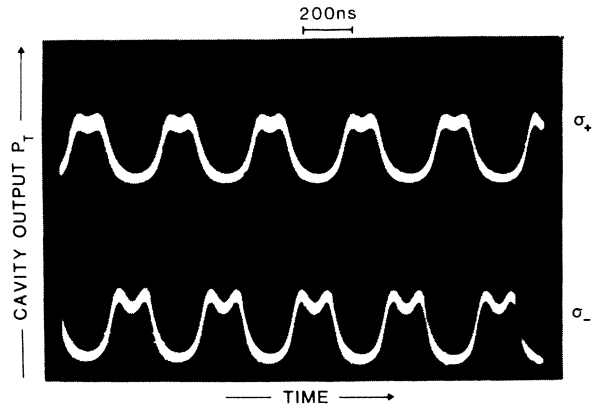

FIG. 8. Magnetically induced self-pulsing on a shorter time scale (200 ns per division; ground lines are at bottom and middle line of graticule, respectively). It can be clearly seen that the two circularly polarized components (σ_+ and σ_-) oscillate with opposite phase.

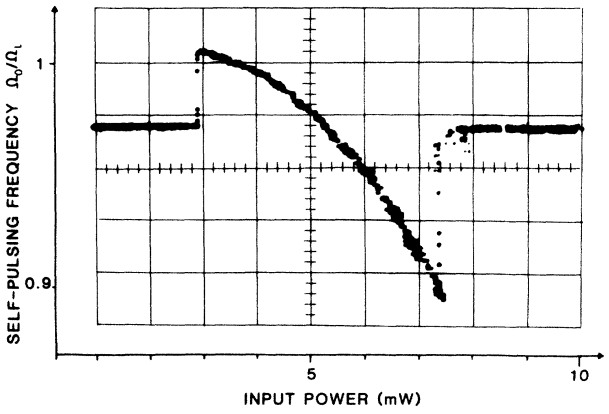

FIG. 9. Measurement of the self-oscillation frequency Ω_0 as a function of input power. The horizontal parts of the curve correspond to the free-running frequency of the PLL and indicate that no self-pulsing is present. The ordinate is displayed in units of the Larmor frequency that was determined from the calibrated magnetic field coils (see text).

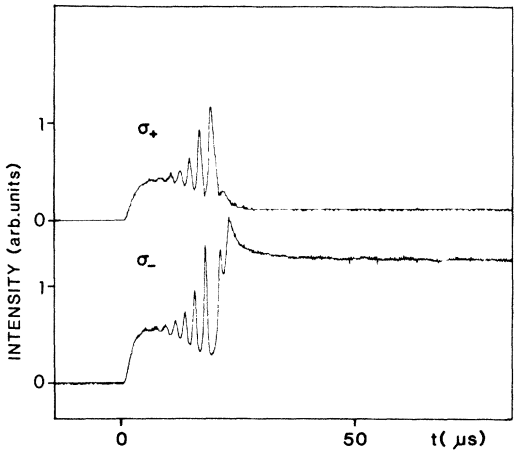

FIG. 11. The stopping of oscilations. With respect to Fig. 10, the input power is slightly increased.

oscillations can be observed in the response to the input step. On the other hand, the intensity at which the oscillations stop and an asymmetric polarization state is reached is increasing roughly proportional with the magnetic field, which is again in agreement with our numerical findings.

We also measured directly the frequency of the self-oscillation as a function of either the input intensity or the cavity tuning by means of a phase-locked loop (PLL) technique. A typical result is shown in Fig. 9; here the oscillation frequency is displayed normalized to the atomic Larmor frequency. The latter one was derived from the calibration factor for the magnetic field coils with the use of the relation $\Omega_L = \mu_B g_F B/\text{mT}$; this calibration factor was determined with the help of a double-resonance technique to a precision of 1%. At high pumping rates, we typically find deviations of Ω_0 from Ω_L of about 10%. The decrease of Ω_0 with increasing pumping rate is in qualitative agreement with Eq. (15) which, of course, cannot predict the high-intensity stopping of the oscillations visible in Fig. 9.

The initial transient shows the same behavior as in the numerical simulations, namely, a monotonous approach to the stationary amplitude for intensities not too far above threshold, an overshooting approach for higher intensities, and finally an approach to an asymmetric fixed point. Examples for this behavior are given in Figs. 10 and 11, respectively. In accord with the numerical findings, we also observe the staggering transients in the experiment which we interpret as chaotic transients. They occur at intensities slightly below the final stopping of the oscillations. After the complicated transient, either a fixed point or the limit cycle may be reached. The latter case is illustrated in Fig. 12.

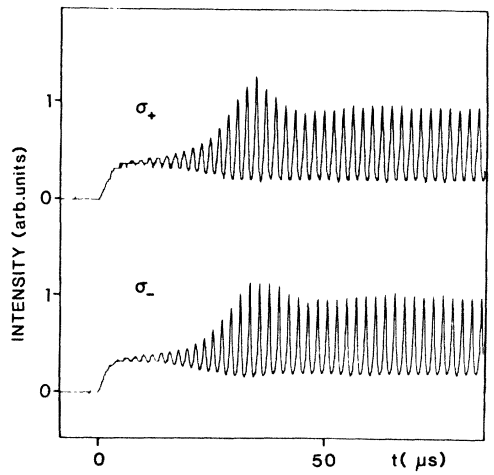

FIG. 10. The onset of self-pulsing. After an initial stage a regular pulse train develops; the oscillation frequency is $\Omega_0/2\pi = 509$ kHz.

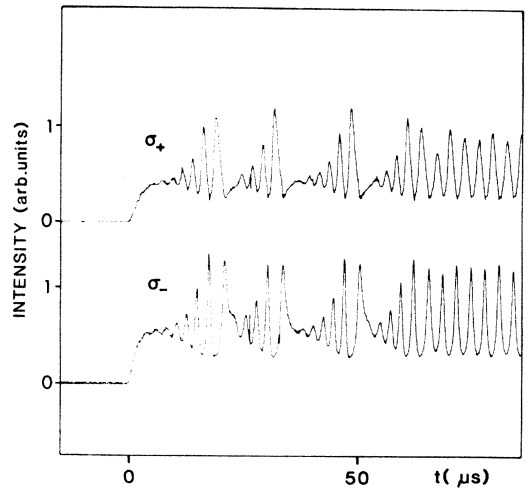

FIG. 12. Experimentally observed staggering transient, here evolving towards a limit cycle. The experimental conditions are nearly identical to those in Fig. 11.

VI. SUMMARY AND OUTLOOK

We have described theory and experimental results of magnetically induced optical self-pulsing in a sodium-filled Fabry-Perot resonator. The oscillation frequency of the device could be tuned from 140 kHz to 13 MHz by simply varying an external static magnetic field. Optical powers of only a few mW from a single-mode laser are sufficient to drive the system. Our experimental findings are found to be in satisfactory agreement with numerical calculations.

It is clear that a sodium experiment is not of immediate interest for technical applications. We would like to emphasize, however, that the phenomenon reported here can occur whenever circularly polarized cavity modes interact via a $J=\frac{1}{2}\rightarrow J'=\frac{1}{2}$ transition in the presence of an external magnetic field. It seems not unreasonable to expect that materials may be found that exhibit the type of limit cycle described here while avoiding the clumsiness of the present setup. As far as possible applications are concerned, the feasibility of an optical data link was already demonstrated;[5] further applications might include an optical modulator, an optical clock, or an optical magnetic field-to-frequency converter. Higher frequencies than our 13 MHz can presumably be generated by making the Larmor frequency equal to the cavity-mode spacing (or an integer multiple of it); this assumption is in fact supported by our numerical calculations. Let us also note that self-sustained spin precession has been predicted in a somewhat similar device that circumvents the restrictions on the upper frequency limit because it does not use an optical cavity.[19] In addition, we may remark that very recently the same type of self-oscillations as described here were also observed in the phase conjugated wave in an intracavity four-wave-mixing experiment.[20]

Finally, we would like to mention that bistable optical devices having a symmetry with respect to the exchange of two circular polarizations have also been discussed in the context of chaos.[15,21] In the experiment reported here no experimental evidence of chaotic behavior was found so far; as pointed out above, it was also not expected in the parameter range studied in this work. What we do see, however, are chaotic transients in both calculation and experiment. For a cavity somewhat longer than the one presently used, our theory predicts the occurrence of sustained chaos: unlike the usual delay-induced instabilities, here the required delay t_R is only very small compared with the relevant time constant of the medium ($t_R\gamma \ll 1$). Experiments are now under way to test these theoretical predictions.

ACKNOWLEDGMENTS

We thank the Deutsche Forschungsgemeinschaft for financial support. One of us (J.M.) acknowledges additional support from the Heisenberg Program.

APPENDIX A: DERIVATION OF THE EQUATIONS OF MOTION

In this Appendix we outline the derivation of Eqs. (2)–(6) presented in Sec. III. We start from the Liouville equation

$$i\hbar\dot{\rho}=[\mathscr{H},\rho]\ . \tag{A1}$$

The Hamiltonian

$$\mathscr{H}=\mathscr{H}_0-\boldsymbol{\mu}_E\cdot\mathbf{E}-\boldsymbol{\mu}_M\cdot\mathbf{B} \tag{A2}$$

contains contributions from both the optical field $\mathbf{E}$ and the static magnetic field $\mathbf{B}$ with $\boldsymbol{\mu}_E$ and $\boldsymbol{\mu}_M$ being the operators of the electric and magnetic dipole moments, respectively. As a quantization axis we choose the z axis that coincides with the propagation direction of the input light field. Using the standard spherical basis, the optical field is written as a monochromatic plane wave:

$$\mathbf{E}(z,t)=\tfrac{1}{2}\sum_q(-1)^q E_q(z)\hat{\mathbf{e}}_{-q}e^{i\omega t}+\text{c.c.}\ , \tag{A3}$$

with $\hat{\mathbf{e}}_\pm=\mp(\hat{\mathbf{e}}_x\pm i\hat{\mathbf{e}}_y)/\sqrt{2}$ and $\hat{\mathbf{e}}_0=\hat{\mathbf{e}}_z$. Here E_+ (E_-) is the field amplitude of the σ_+ (σ_-) polarized component of the light field and $E_0=0$.

The Hamiltonian satisfies the usual conditions:

$$\langle i\,|\,\mathscr{H}_0\,|\,j\rangle=\hbar\omega_{ij}\delta_{ij},\quad \langle i\,|\,-\boldsymbol{\mu}_E\cdot\mathbf{E}-\boldsymbol{\mu}_M\cdot\mathbf{B}\,|\,i\rangle=0\ ,$$
$$i,j=1,2,3,4\ .$$

The atomic transition frequency is defined by $\omega_3-\omega_1=\omega_0$. The matrix elements of $\boldsymbol{\mu}_E\cdot\mathbf{E}$ are given by

$$\frac{1}{\hbar}\langle 3\,|\,-\boldsymbol{\mu}_E\cdot\mathbf{E}\,|\,2\rangle=\beta_+e^{i\omega t}-\beta_-^*e^{-i\omega t}\ , \tag{A4}$$

$$\frac{1}{\hbar}\langle 4\,|\,-\boldsymbol{\mu}_E\cdot\mathbf{E}\,|\,1\rangle=-\beta_-e^{i\omega t}+\beta_+^*e^{-i\omega t}\ , \tag{A5}$$

with $\beta_\pm$ denoting the electric dipole coupling strength with respect to the $\sigma_\pm$ transition:

$$\beta_\pm=\mu_E E_\pm/2\hbar\ . \tag{A6}$$

Here μ_E is the reduced electric dipole matrix element. The magnetic dipole matrix elements can be also easily calculated:

$$\frac{1}{\hbar}\langle 2\,|\,-\boldsymbol{\mu}_M\cdot\mathbf{B}\,|\,1\rangle=\tfrac{1}{2}\Omega_L\ , \tag{A7}$$

$$\frac{1}{\hbar}\langle 4\,|\,-\boldsymbol{\mu}_M\cdot\mathbf{B}\,|\,3\rangle=\tfrac{1}{2}\Omega_L'\ . \tag{A8}$$

Here $\Omega_L=\mu_B g_J B/\hbar$ and $\Omega_L'=\mu_B g_{J'}B/\hbar$ describe the Larmor frequencies of the ground state and excited state, respectively; μ_B is the Bohr magneton and g_J denotes the Landé factor.

We now phenomenologically introduce the following decay times: τ_1 and τ_2 denote the decay of the ground-state population difference $\rho_{11}-\rho_{22}$ and of the coherence ρ_{12}, respectively. Correspondingly, τ_1' and τ_2' describe the decay of $\rho_{33}-\rho_{44}$ and of the excited-state coherence ρ_{34}. T_1 is the excited-state lifetime and T_2 the decay time of the optical coherences. By defining $\Delta=\omega_0-\omega$ and

$$\rho_{ij}=\tilde{\rho}_{ij}e^{-i\omega t},\quad i=3,4,\ j=1,2 \tag{A9}$$

and applying the rotating-wave approximation (RWA), the equations of motions for the density-matrix elements become

$$\dot{\rho}_{11}=i(\rho_{12}-\rho_{21})\frac{\Omega_L}{2}+i(\beta_+^*\tilde{\rho}_{14}-\beta_+\tilde{\rho}_{41})$$
$$-\frac{1}{2\tau_1}(\rho_{11}-\rho_{22})+\frac{1}{2T_1}(\rho_{33}+\rho_{44}) , \quad \text{(A10)}$$

$$\dot{\rho}_{22}=-i(\rho_{12}-\rho_{21})\frac{\Omega_L}{2}+i(\beta_-\tilde{\rho}_{32}-\beta_-^*\tilde{\rho}_{23})$$
$$+\frac{1}{2\tau_1}(\rho_{11}-\rho_{22})+\frac{1}{2T_1}(\rho_{33}+\rho_{44}) , \quad \text{(A11)}$$

$$\dot{\rho}_{33}=i(\rho_{34}-\rho_{43})\frac{\Omega_L'}{2}-i(\beta_-\tilde{\rho}_{32}-\beta_-^*\tilde{\rho}_{23})$$
$$-\frac{1}{2\tau_1'}(\rho_{33}-\rho_{44})-\frac{1}{T_1}\rho_{33} , \quad \text{(A12)}$$

$$\dot{\rho}_{44}=-i(\rho_{34}-\rho_{43})\frac{\Omega_L'}{2}-i(\beta_+^*\tilde{\rho}_{14}-\beta_+\tilde{\rho}_{41})$$
$$+\frac{1}{2\tau_1'}(\rho_{33}-\rho_{44})-\frac{1}{T_1}\rho_{44} , \quad \text{(A13)}$$

$$\dot{\rho}_{12}=i(\rho_{11}-\rho_{22})\frac{\Omega_L}{2}-i(\beta_+\tilde{\rho}_{42}+\beta_-^*\tilde{\rho}_{13})-\frac{1}{\tau_2}\rho_{12} , \quad \text{(A14)}$$

$$\dot{\rho}_{34}=i(\rho_{33}-\rho_{44})\frac{\Omega_L'}{2}+i(\beta_-^*\tilde{\rho}_{24}+\tilde{\rho}_{31}\beta_+)-\frac{1}{\tau_2'}\rho_{34} , \quad \text{(A15)}$$

$$\dot{\tilde{\rho}}_{13}=\left[i\Delta-\frac{1}{T_2}\right]\tilde{\rho}_{13}-i\left[\frac{\Omega_L}{2}\tilde{\rho}_{23}-\frac{\Omega_L'}{2}\tilde{\rho}_{14}\right]$$
$$-i(\beta_+\rho_{43}+\beta_-\rho_{12}) , \quad \text{(A16)}$$

$$\dot{\tilde{\rho}}_{14}=\left[i\Delta-\frac{1}{T_2}\right]\tilde{\rho}_{14}-i\left[\frac{\Omega_L}{2}\tilde{\rho}_{24}-\frac{\Omega_L'}{2}\tilde{\rho}_{13}\right]$$
$$+i\beta_+(\rho_{11}-\rho_{44}) , \quad \text{(A17)}$$

$$\dot{\tilde{\rho}}_{23}=\left[i\Delta-\frac{1}{T_2}\right]\tilde{\rho}_{23}-i\left[\frac{\Omega_L}{2}\tilde{\rho}_{13}-\frac{\Omega_L'}{2}\tilde{\rho}_{24}\right]$$
$$-i\beta_-(\rho_{22}-\rho_{33}) , \quad \text{(A18)}$$

$$\dot{\tilde{\rho}}_{24}=\left[i\Delta-\frac{1}{T_2}\right]\tilde{\rho}_{24}-i\left[\frac{\Omega_L}{2}\tilde{\rho}_{14}-\frac{\Omega_L'}{2}\tilde{\rho}_{23}\right]$$
$$+i(\beta_-\rho_{34}+\beta_+\rho_{21}) . \quad \text{(A19)}$$

With respect to our experimental situation, the equations of motion (A10)–(A19) can be considerably simplified. Under conditions of high buffer gas pressure, the excited-state sublevel coherence ρ_{34} and the excited-state population difference $\rho_{33}-\rho_{44}$ are rapidly destroyed due to collisions; thus we assume $\rho_{34}\simeq 0$ and $\rho_{33}-\rho_{44}\simeq 0$. On the other hand, the atomic ground state is rather insensitive to collisions. In fact, the relaxation of ρ_{12} and $\rho_{11}-\rho_{22}$ is due to diffusive motion of the atoms through the laser beam; thus we set $\tau_1=\tau_2$. Moreover, in our experiment the inequality $\Omega_L,\Omega_L' \ll 1/T_2$ is fulfilled ($\Omega_L,\Omega_L' \leq 10^8\ \mathrm{s}^{-1}$, $T_2\simeq 10^{-10}$ s); consequently, we neglect the terms proportional to Ω_L and Ω_L' in Eqs. (A16)–(A19).

In the experiment, τ_1 is about 10 μs, i.e., ρ_{12} and $\rho_{11}-\rho_{22}$ are only slowly time dependent in comparison with the fast time variations of the optical coherences ($T_2\simeq 10^{-10}$ s). As a consequence, Eq. (A16)–(A19) can be integrated; this procedure is also known as adiabatic elimination of the optical coherences. If we finally assume small light intensities, we can neglect the populations in the excited state. By setting ρ_{33} and ρ_{44} equal to zero, Eqs. (A16)–(A19) yield

$$\tilde{\rho}_{13}=\frac{\beta_-}{\Delta+i/T_2}\rho_{12} , \quad \text{(A20)}$$

$$\tilde{\rho}_{14}=\frac{-\beta_+}{\Delta+i/T_2}\rho_{11} , \quad \text{(A21)}$$

$$\tilde{\rho}_{23}=\frac{\beta_-}{\Delta+i/T_2}\rho_{22} , \quad \text{(A22)}$$

$$\tilde{\rho}_{24}=\frac{-\beta_+}{\Delta+i/T_2}\rho_{21} . \quad \text{(A23)}$$

By defining

$$\frac{1}{\tau_1}=\gamma, \quad \frac{1}{T_2}=\Gamma_2, \quad \bar{\Delta}=\Delta/\Gamma_2, \quad P_\pm=\frac{1}{\Gamma_2}\frac{|\beta_\pm|^2}{\bar{\Delta}^2+1} \quad \text{(A24)}$$

and

$$u=\rho_{12}+\rho_{21}, \quad v=i(\rho_{12}-\rho_{21}), \quad w=\rho_{11}-\rho_{22} \quad \text{(A25)}$$

one obtains the following equations of motion for the ground-state variables:

$$\dot{u}=-(P_++P_-+\gamma)u-(P_--P_+)\bar{\Delta}v , \quad \text{(A26a)}$$

$$\dot{v}=-(P_++P_-+\gamma)v+(P_--P_+)\bar{\Delta}u-\Omega_L w , \quad \text{(A26b)}$$

$$\dot{w}=-(P_++P_-+\gamma)w+\Omega_L v+(P_--P_+) . \quad \text{(A26c)}$$

Equations (A26a)–(A26c) can be also written as a Bloch equation [see Eq. (4)].

The optical polarization of the medium is given by

$$\mathscr{P}(z,t)=\tfrac{1}{2}\sum_q(-1)^q\mathscr{P}_q\hat{\mathbf{e}}_{-q}e^{i\omega t}+\text{c.c.}=N\,\mathrm{Tr}(\boldsymbol{\mu}_E\rho) , \quad \text{(A27)}$$

with N denoting the atomic number density. We are especially interested in the polarization components $\mathscr{P}_\pm$. With the use of Eqs. (A21) and (A22) and the relations $\rho_{11}=\frac{1}{2}(1+w)$ and $\rho_{22}=\frac{1}{2}(1-w)$, we find

$$\mathscr{P}_\pm=\frac{N\mu_E^2}{2\hbar\Gamma_2}\frac{\bar{\Delta}-i}{\bar{\Delta}^2+1}(1\pm w)E_\pm=\epsilon_0\chi_\pm E_\pm . \quad \text{(A28)}$$

Here, $\chi_\pm$ denotes the susceptibility of the medium with respect to the $\sigma_\pm$ component. For a dilute sample the approximation $(1+\chi_\pm)^{1/2}\simeq 1+\chi_\pm/2$ holds and we finally obtain for the index of refraction $n_\pm$ and the absorption coefficient $\alpha_\pm$:

$$n_\pm = 1+\tfrac{1}{2}\mathrm{Re}\chi_\pm = 1+(n_0-1)(1\pm w)\ , \tag{A29}$$

$$\alpha_\pm = -\frac{\omega}{2c}\mathrm{Im}\chi_\pm = \alpha_0(1\pm w)\ , \tag{A30}$$

with

$$n_0 = 1+\frac{N\mu_E^2}{4\hbar\epsilon_0\Gamma_2}\frac{\bar{\Delta}}{\bar{\Delta}^2+1}\ , \tag{A31}$$

$$\alpha_0 = \frac{N\mu_E^2\omega}{4\hbar\epsilon_0 c\Gamma_2}\frac{1}{\bar{\Delta}^2+1}\ . \tag{A32}$$

APPENDIX B: THE RESONATOR EQUATION

In deriving the resonator equation (7) we closely follow a theoretical approach outlined by Ikeda in Ref. 11. For this purpose we consider a ring cavity (see Fig. 13) with partially reflecting input and output mirrors having intensity reflection coefficients R_f and R_b, respectively; the mirrors which close the optical path are perfectly reflecting. L is the length of the sample, and $\mathcal{L}=L+l$ is the total physical length of the optical path in the cavity. Let $E_\pm(t,z)$ be the complex envelope of the electric field (A3). Then the following boundary conditions on the amplitudes are required:

$$E_\pm(t,0) = \sqrt{1-R_f}E_{I,\pm}(t) + \sqrt{R_fR_b}e^{-ik\mathcal{L}}E_\pm(t-l/c,L)\ , \tag{B1}$$

$$E_{T,\pm}(t) = \sqrt{1-R_b}E_\pm(t,L)e^{-ikL}\ . \tag{B2}$$

Here, E_I and E_T denote the incident and transmitted field, respectively. In the slowly varying amplitude approximation, the field distribution in the medium is given by

$$\frac{dE_\pm(t',z)}{dz} = -\tfrac{1}{2}ik\chi_\pm(t',z)E_\pm(t',z)\ , \tag{B3}$$

with $\chi_\pm(t',z)$ being defined by Eq. (A28). $\chi_\pm$ depends on t' via the time dependence of w and it also depends on z because w is a function of $|E_\pm(t',z)|^2$ [see Eq. (A26)]. By introducing the retarded time $\tau=t'-z/c$, we can write Eq. (B3) in the following integral form:

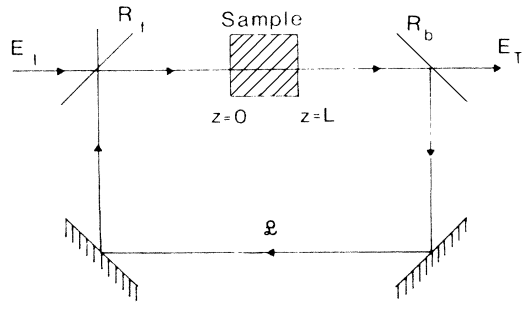

FIG. 13. The ring resonator (see text).

$$E_\pm(\tau+z/c,z) = E_\pm(\tau,0)\exp[-\tfrac{1}{2}ikW_\pm(\tau,z)]\ , \tag{B4}$$

with

$$W_\pm(\tau,z) = \int_0^z \chi_\pm(\tau+z'/c,z')dz' = \frac{N\mu_E^2}{2\hbar\Gamma_2\epsilon_0}\frac{\bar{\Delta}-i}{\bar{\Delta}^2+1}\left[z\pm\int_0^z w(\tau+z'/c,z')dz'\right]\ . \tag{B5}$$

The time dependence of $W_\pm(\tau,z)$ is given by Eq. (A26c). Combining Eqs. (B4) and (B5) with the boundary condition (B1) and defining $t=\tau+\mathcal{L}/c$, we obtain an equation not involving the spatial coordinate:

$$E_\pm(t,0) = \sqrt{1-R_f}E_I(t) + \sqrt{R_fR_b}e^{-ik\mathcal{L}}E_\pm(t-\mathcal{L}/c,0)\times\exp[-\tfrac{1}{2}ikW_\pm(t-\mathcal{L}/c,L)]\ . \tag{B6}$$

The integral $W_\pm$ in Eq. (B6) can easily be calculated if the spatial dependence of w over the sample length can be neglected, i.e., if we assume an optically and physically thin sample. More specifically, we set $w(t-\mathcal{L}/c+z'/c,z')=w(t-\mathcal{L}/c,0)\equiv w(t-\mathcal{L}/c)$. Implicitly, we thus also set $|E_\pm(z')|^2=|E_\pm(z'=0)|^2$; this is essentially the basis of the well-known mean-field theories of optical bistability.[22] $W_\pm$ then yields

$$W_\pm(t-\mathcal{L}/c,L)\simeq\frac{N\mu_E^2}{2\hbar\Gamma_2\epsilon_0}\frac{\bar{\Delta}-i}{\bar{\Delta}^2+1}[1\pm w(t-\mathcal{L}/c)]L\ . \tag{B7}$$

With the use of the definition

$$p_\pm(t) = \left[\frac{1}{\Gamma_2}\frac{1}{\bar{\Delta}^2+1}\right]^{1/2}\frac{\mu_E}{2\hbar}E_\pm(t)\ , \tag{B8}$$

Eq. (B6) can now be written as

$$p_\pm(t) = \sqrt{1-R_f}p_{I,\pm}(t)+\sqrt{R_fR_b}p_\pm(t-t_R)\times\exp[-L\alpha_\pm(t-t_R) - i\phi_\pm(t-t_R)-i\phi_0]\ . \tag{B9}$$

Here, $t_R=\mathcal{L}/c$ is the resonator round-trip time, $\phi_0=kl-2\pi M$ and $\phi_\pm=kLn_\pm$; $\alpha_\pm$ and $n_\pm$ are given by Eqs. (A31) and (A32). The transmitted field amplitude can easily be calculated by using the boundary condition (B2). We note that Eqs. (B9) and (A26) can be interpreted as difference-differential equations.

Equation (B9) considerably simplifies if propagation effects can be neglected. In our case, this is justified if the following inequalities hold:

$$t_R\gamma\ll 1,\quad t_R\Omega_L\ll 1,\quad t_RP_\pm\ll 1\ ,\quad t_R\left|\frac{\partial E_\pm(t-t_R)}{\partial t}\right|\ll 1\ . \tag{B10}$$

Under these conditions we can set $E_\pm(t)=E_\pm(t-t_R)$ and $W_\pm(t)=W_\pm(t-t_R)$. The resonator equation (B9) then transforms into an Airy function for the intracavity pump rate $P_\pm(t)=|p_\pm(t)|^2$. By straightforward calculation from (B9) one finds

$$P_{\pm}(t)=P_{I,\pm}(t)\frac{(1-R_f)}{[1-R_{\rm eff}(t)]^2}\frac{1}{\{1+4R_{\rm eff}(t)/[1-R_{\rm eff}(t)]^2\}\sin^2\{\frac{1}{2}[\phi_{\pm}(t)+\phi_0]\}}\ , \tag{B11}$$

with

$$R_{\rm eff}(t)=\sqrt{R_f R_b}\,e^{-\alpha_{\pm}(t)L}\ . \tag{B12}$$

Equation (B11) is used in the stability analysis in Sec. III C.

[1]S. L. McCall, Appl. Phys. Lett. **32**, 284 (1977).

[2]M. Cheung, S. D. Durbin, and Y. R. Shen, Opt. Lett. **8**, 39 (1983).

[3]J. L. Jewell, H. M. Gibbs, S. S. Tarng, A. C. Gossard, and W. Wiegmann, Appl. Phys. Lett. **40**, 291 (1982).

[4]M. Kitano, T. Yabuzaki, and T. Ogawa, Phys. Rev. A **24**, 3156 (1981).

[5]F. Mitschke, J. Mlynek, and W. Lange, Phys. Rev. Lett. **50**, 1660 (1983).

[6]F. T. Arecchi, G. Giusfredi, E. Petriella, and P. Salieri, Appl. Phys. B **29**, 79 (1982).

[7]M. Kitano, T. Yabuzaki, and T. Ogawa, Phys. Rev. Lett. **46**, 926 (1980).

[8]S. Cecchi, G. Giusfredi, E. Petriella, and P. Salieri, Phys. Rev. Lett. **49**, 1928 (1982).

[9]M. W. Hamilton, W. J. Sandle, J. T. Chilwell, J. S. Satchell, and D. M. Warrington, Opt. Commun. **48**, 190 (1983).

[10]J. Mlynek, S. Burschka, and E. Buhr (unpublished).

[11]K. Ikeda, Opt. Commun. **30**, 257 (1979); J. Phys. (Paris) Colloq. **44**, C2-183 (1983).

[12]F. Mitschke, Ph.D. thesis, University of Hannover, 1984.

[13]T. Shimizu and N. Morioka, Phys. Lett. **69A**, 148 (1978).

[14]J. A. Yorke and E. D. Yorke, J. Stat. Phys. **21**, 263 (1979).

[15]M. Kitano, T. Yabuzaki, and T. Ogawa, Phys. Rev. A **29**, 1288 (1984).

[16]See, e.g., L. C. Balling, in *Advances in Quantum Electronics*, edited by D. W. Goodwin (Academic, New York, 1975), Vol. 3, p. 1.

[17]E. Köster, J. Mlynek, and W. Lange, Opt. Commun. **53**, 53 (1985).

[18]J. Mlynek, F. Mitschke, R. Deserno, and W. Lange, Phys. Rev. A **29**, 1297 (1984).

[19]M. Kitano, T. Yabuzaki, and T. Ogawa, Phys. Rev. A **29**, 1964 (1984).

[20]E. Köster, J. Kolbe, F. Mitschke, J. Mlynek, and W. Lange, Appl. Phys. B **35**, 201 (1984).

[21]H. J. Carmichael, C. M. Savage, and D. F. Walls, Phys. Rev. Lett. **50**, 163 (1983).

[22]H. J. Carmichael and J. A. Hermann, Z. Phys. B **38**, 365 (1980).

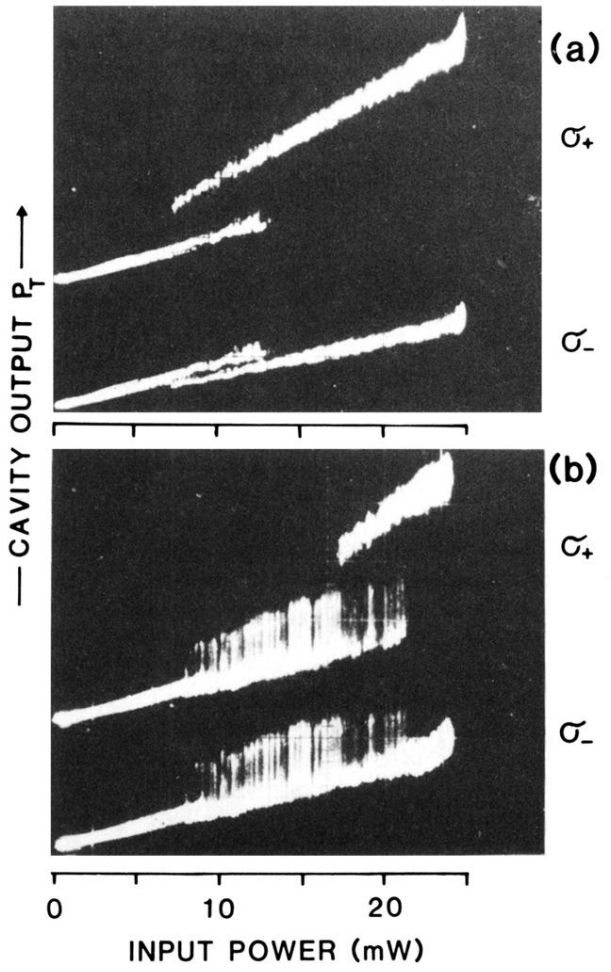

FIG. 7. Experimental recordings of hysteresis cycles as the input power is scanned forth and back. The ordinate displays the signals of the two photodiodes PD_1 and PD_2 which monitor the σ_+ and σ_- components of the cavity output, respectively; the two traces are separated vertically for clearness. (a) No magnetic field applied. (b) $B=0.06$ mT $[\Omega_L=2\pi(400\text{ kHz})]$; the self-oscillations appear as shaded area. Other experimental parameters in (a) and (b) are $\Delta\simeq 2\pi(5\text{ GHz})$, $N_{Na}\simeq 10^{12}\text{ cm}^{-3}$, and $p_{Ar}\simeq 200$ mbar; linear input polarization.

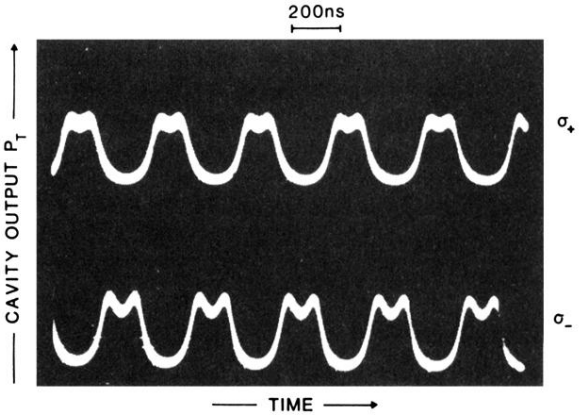

FIG. 8. Magnetically induced self-pulsing on a shorter time scale (200 ns per division; ground lines are at bottom and middle line of graticule, respectively). It can be clearly seen that the two circularly polarized components (σ_+ and σ_-) oscillate with opposite phase.